Enantioselective responses in Compton scattering of chiral hydrogen

Dejia Dai [1], Chong Ye [2,*], and Libin Fu [1,†]

[1]*Graduate School of China Academy of Engineering Physics, Beijing 100193, China*
[2]*Beijing Key Laboratory of Nanophotonics and Ultrafine Optoelectronic Systems School of Physics, Beijing Institute of Technology, Beijing 100081, China*

The study of chiral molecules using Compton scattering is an area that holds promise for further exploration. The current paper presents a preliminary and relatively simple discussion on the possibility of applying Compton ionization to enantiomeric recognition. By focusing on two different types of chiral hydrogen, we find that the momentum spectrum of Compton electrons can encode chiral features, whereas the light-scattering spectra may not necessarily do so. In particular, the momentum spectrum can also exhibit chirality. These results could provide valuable insights and recommendations for the investigation of actual chiral molecules.

I. INTRODUCTION

It is extremely important to understand the microstructure of matter. To this end, modern science has developed various detection techniques, among which the application of x rays plays a key role [1]. As a probe based on electromagnetic interaction, x rays are widely used in crystal structure determination [2], atomic and molecular structure research [3], plasma diagnostics [4], ultrafast imaging of electron motion [5,6], and other fields.

Compton scattering [7,8] is one of the physical mechanisms of x-ray interactions with matter. It has a significant advantage in determining the momentum distribution of bound electrons [3] and the corresponding fundamental principle is the impulse approximation (IA) [9,10]. On the basis of this approximation, a bound electron can be considered to be in a free state when the energy transferred by the photon is much greater than its binding energy. Consequently, the electron's momentum distribution is encoded in the light-scattering spectra in a very simple form. Nevertheless, little attention has been paid to the application value of physical quantities other than the light-scattering spectra in the Compton scattering process since the inception of the IA. Recently, based on the kinematically complete experiments [11,12] of Compton scattering, some studies [13,14] discussed the possibility of using Compton ionization as a method of dynamic spectroscopy. The central idea involves employing the cold target recoil ion momentum spectroscopy (COLTRIMS) technique [15,16] to perform coincidence measurement of the momentum of Compton electrons and ion fragments, enabling the reconstruction of physical characteristics of the target atoms or molecules. This indicates that in the process of Compton ionization, in comparison to the light-scattering spectra, the momentum spectrum of electrons or ions is also rich in structural information about the target.

On the other hand, chirality is one of the structural characteristics of molecules. Molecules of different chirality are also called enantiomers. They share most of their physical properties. Yet, they play significantly different roles in broad classes of chemical reactions, biological activity, and the function of drugs. Therefore, the effective detection of molecular chirality is of paramount significance in the fields of medicine, pharmaceuticals, and biochemistry. Currently, methods based on the interaction of light with matter, such as circular dichroism spectroscopy [17–19], optical rotatory dispersion [17–19], Coulomb explosion imaging [20], three-wave mixing [21–23], and enantioselective high-order harmonic generation (HHG) [24,25], have been employed for enantiomer identification. Compared with these methods, Compton scattering is expected to be used to reconfigure the state of bound electrons, which is inherently chiral in chiral molecules. But to our surprise, the application of Compton scattering in this regard has seen scarce discussion and research.

In this paper, we explore the possibility of reading out the chirality of bound electrons by using Compton scattering. For simplicity, we focus on the case of chiral hydrogenic wave functions [26], which were recently introduced as a tool to explore the basic physical mechanisms underlying the chiral response at the level of electrons. For chiral hydrogen with a given spatial orientation, we will focus on analyzing the light-scattering spectra and the momentum spectrum of Compton electrons. Our results will demonstrate the superiority of the momentum spectrum of Compton electrons in distinguishing enantiomers compared to the light-scattering spectra. The chiral hydrogenic wave functions can be realized in atoms by using synthetic chiral light fields [27]. In this context, our work can have an impact on the related area soon or in the near future.

The paper is organized as follows. In Sec. II, the theoretical methods are described in detail. In Sec. III, our numerical results are presented. We summarize and discuss in Sec. IV.

*yechong@bit.edu.cn
†lbfu@gscaep.ac.cn

Unless stated otherwise, atomic units (a.u.) with $m_e = \hbar = e = 1$ and $c \approx 137.036$ are employed throughout this paper. Here, e represents the elementary charge and c is the speed of light. m_e refers to the mass of the electron.

II. METHODS

A. The fundamental description of the Compton scattering of chiral hydrogen

By neglecting the nuclear motion effects, the Hamiltonian of the hybrid system of a single-electron atom and x rays can be written as

$$H = \frac{(\boldsymbol{p} + \boldsymbol{A})^2}{2} + V_c(\boldsymbol{r}) + \sum_{\boldsymbol{q},\epsilon} \omega_q a_{\boldsymbol{q},\epsilon} a_{\boldsymbol{q},\epsilon}^\dagger, \qquad (1)$$

where

$$\boldsymbol{A} = \sum_{\boldsymbol{q},\epsilon} \sqrt{\frac{2\pi}{\omega_q V}} (e^{i\boldsymbol{q}\cdot\boldsymbol{r}} \epsilon a_{\boldsymbol{q},\epsilon} + \text{H.c.}). \qquad (2)$$

In the above equations, ϵ and $\boldsymbol{q}$ represent the polarization vector and wave vector of the photon, respectively. Here, the Coulomb gauge is employed, hence $\boldsymbol{q} \cdot \epsilon = 0$. The annihilation operator for photons is given as $a_{\boldsymbol{q},\epsilon}$. The angular frequency of the photon is given as $\omega = c|\boldsymbol{q}|$. V is the normalized volume of the light field, and we can conveniently set it to 1. $V_c(\boldsymbol{r}) = -1/r$ represents the Coulomb potential energy.

Thus, the interaction term is

$$H_I = \boldsymbol{p} \cdot \boldsymbol{A} + \frac{\boldsymbol{A}^2}{2}. \qquad (3)$$

When Compton scattering occurs, the initial state ϕ_i and final state ϕ_f of the system are as follows,

$$\phi_i = \psi_0(\boldsymbol{r}) \otimes |1_{\boldsymbol{k}_1}\rangle \otimes |0_{\boldsymbol{k}_2}\rangle \, e^{-i(E_0 + \omega_1)t},$$

$$\phi_f = \psi_{\boldsymbol{p}}(\boldsymbol{r}) \otimes |0_{\boldsymbol{k}_1}\rangle \otimes |1_{\boldsymbol{k}_2}\rangle \, e^{-i(E_f + \omega_2)t}. \qquad (4)$$

Here, $\boldsymbol{k}_1$ and $\boldsymbol{k}_2$ are the wave vectors of the incident and scattered photons, respectively. $\psi_0(\boldsymbol{r})$ is the wave function for a bound electron in the atom and E_0 is the corresponding energy eigenvalue. $\psi_{\boldsymbol{p}}(\boldsymbol{r})$ is the Coulomb wave function and $E_f = p^2/2$. For the chiral hydrogen [26], there are

$$\psi_0(\boldsymbol{r}) = \sum_{(nlm)} R_{nlm}(r) Y_{lm}(\hat{\boldsymbol{r}}) \qquad (5)$$

and $E_0 = -1/(2n^2)$, where $Y_{lm}(\hat{\boldsymbol{r}})$ is the spherical harmonic and $\hat{\boldsymbol{r}}$ represents the solid angle. $R_{nlm}(r)$ refers to the radial wave function. Note that the parentheses below the summation symbol indicate that nlm represents a single variable index.

We only consider the A^2 term in the interaction, which is the so-called A^2 approximation. This approximation is highly valid in the nonrelativistic Compton scattering of atoms [9]. As a result, the differential cross section for Compton scattering of chiral hydrogen is given by

$$d\sigma = \frac{|\epsilon_1 \cdot \epsilon_2|^2}{\omega_1 \omega_2} |M|^2 \delta(\omega_1 + E_0 - \omega_2 - E_f) d\boldsymbol{k}_2 d\boldsymbol{p}, \qquad (6)$$

where ϵ_1 and ϵ_2 are the polarization vectors of incident photons and scattered photons, respectively, and the matrix element M is given by the following expression,

$$M = \langle \psi_{\boldsymbol{p}} | e^{i\boldsymbol{k}\cdot\boldsymbol{r}} \mathcal{S}(\alpha, \beta, \gamma) | \psi_0 \rangle$$

$$= \sum_{(nlm)m'} D_{m'm}^l(\alpha, \beta, \gamma) \langle \psi_{\boldsymbol{p}} | e^{i\boldsymbol{k}\cdot\boldsymbol{r}} | \psi_{lmm'} \rangle. \qquad (7)$$

In Eq. (7), $\mathcal{S}(\alpha, \beta, \gamma)$ is the spatial rotation operator acting on the wave function $\psi_0(\boldsymbol{r})$, with α, β, and γ representing the three Euler angles. It is introduced for the convenience of discussing the space orientation of chiral hydrogen in the subsequent text. $\boldsymbol{k} = \boldsymbol{k}_1 - \boldsymbol{k}_2$, which is the transferred momentum from the incident photon to the chiral hydrogen. $\psi_{lmm'}(\boldsymbol{r}) = R_{nlm}(r) Y_{lm'}(\hat{\boldsymbol{r}})$. $D_{m'm}^l(\alpha, \beta, \gamma)$ is the Wigner D-matrix element [28]. For convenience, we will abbreviate $D_{m'm}^l(\alpha, \beta, \gamma)$ as $D_{m'm}^l$ later in this paper.

Now, the key is how to calculate the matrix element $\langle \psi_{\boldsymbol{p}} | e^{i\boldsymbol{k}\cdot\boldsymbol{r}} | \psi_{lmm'} \rangle$. First, through series expansion, we obtain

$$e^{i\boldsymbol{k}\cdot\boldsymbol{r}} = 4\pi \sum_{l_1=0}^{\infty} \sum_{m_1=-l_1}^{l_1} i^{l_1} j_{l_1}(kr) Y_{l_1 m_1}^*(\hat{\boldsymbol{k}}) Y_{l_1 m_1}(\hat{\boldsymbol{r}}) \qquad (8)$$

and

$$\psi_{\boldsymbol{p}}(\boldsymbol{r}) = \frac{4\pi}{pr} \sum_{l_2=0}^{\infty} \sum_{m_1=-l_2}^{l_2} i^{l_2} e^{-i\sigma_{l_2}} F_{l_2}(r) Y_{l_2 m_2}^*(\hat{\boldsymbol{p}}) Y_{l_2 m_2}(\hat{\boldsymbol{r}}). \qquad (9)$$

Here, j_{l_1} is the spherical Bessel function of the first kind. σ_{l_2} is called the Coulomb phase shift and it is given by

$$\sigma_{l_2} = \arg[\Gamma(l_2 + 1 - i/p)]. \qquad (10)$$

$F_{l_2}(r)$ represents the Schrödinger-Coulomb function, which satisfies the following equation,

$$-\frac{1}{2} \frac{d^2 F_{l_2}}{dr^2} + \left[V_c(r) + \frac{l_2(l_2+1)}{2r^2} \right] F_{l_2} = E_f F_{l_2}. \qquad (11)$$

Substituting Eqs. (8) and (9) into Eq. (7) yields

$$M = \sum_{(nlm)l_1 l_2 m_1 m_2 m'} \mathscr{A}\mathscr{B} D_{m'm}^l Y_{l_2 m_2}(\hat{\boldsymbol{p}}), \qquad (12)$$

where

$$\mathscr{A} = (-1)^{m_2} \sqrt{\frac{(2l_1+1)(2l_2+1)(2l+1)}{4\pi}}$$

$$\times \begin{pmatrix} l_2 & l_1 & l \\ 0 & 0 & 0 \end{pmatrix} \begin{pmatrix} l_2 & l_1 & l \\ -m_2 & m_1 & m' \end{pmatrix} \qquad (13)$$

and

$$\mathscr{B} = 16\pi^2 (-1)^{l_2} i^{(l_1+l_2)} e^{i\sigma_{l_2}} Y_{l_1 m_1}^*(\hat{\boldsymbol{k}})/p$$

$$\times \int_0^{\infty} F_{l_2}(r) R_{nlm}(r) j_{l_1}(kr) r \, dr. \qquad (14)$$

In Eq. (13), we employed the Wigner 3-j symbols. In addition, because the integral in Eq. (14) cannot be given by an elementary function, we choose to perform numerical processing on it. Specifically, we first solved Eq. (11) numerically using the code package RADIAL [29] to obtain the function $F_{l_2}(r)$. Subsequently, in accordance with the convergence properties of the radial wave function $R_{nlm}(r)$, we truncated the upper limit of the integral. Ultimately, the numerical integration

result was obtained through the 20-point Gaussian-Legendre quadrature.

Then, we can derive the expression for the light-scattering spectrum by combining Eqs. (5) and (6), that is,

$$\frac{d\sigma}{d\Omega_{\hat{k}_2}d\omega_2} = |\boldsymbol{\epsilon}_1 \cdot \boldsymbol{\epsilon}_2|^2 \frac{p\omega_2}{\omega_1} \sum_{l_2 m_2} \left| \sum_{(nlm)l_1 m_1 m'} D^l_{m'm} \mathscr{A} \mathscr{B} \right|^2, \quad (15)$$

where

$$p = \sqrt{2(\omega_1 + E_0 - \omega_2)}. \quad (16)$$

In Eq. (15), we utilize the orthogonality of spherical harmonics:

$$\int_0^{2\pi} \int_0^{\pi} Y^*_{l_2 m_2}(\hat{\boldsymbol{p}}) Y_{l'_2 m'_2}(\hat{\boldsymbol{p}}) d\Omega_{\hat{p}} = \delta_{l_2 l'_2} \delta_{m_2 m'_2}. \quad (17)$$

Similarly, the momentum spectrum $\varphi(\boldsymbol{p})$ of the ionized electron is given by

$$\varphi(\boldsymbol{p}) = \frac{\mathrm{d}^3\sigma}{\mathrm{d}p_x \mathrm{d}p_y \mathrm{d}p_z} = \int \frac{\omega_2}{\omega_1} |\boldsymbol{\epsilon}_1 \cdot \boldsymbol{\epsilon}_2|^2$$

$$\times \left| \sum_{(nlm)l_1 l_2 m_1 m_2 m'} \mathscr{A} \mathscr{B} D^l_{m'm} Y_{l_2 m_2}(\hat{\boldsymbol{p}}) \right|^2 d\Omega_{\hat{k}_2}, \quad (18)$$

where

$$\omega_2 = \omega_1 + E_0 - p^2/2. \quad (19)$$

B. Remarks on photon polarization

Reviewing the above derivations, we retained the polarization of both incident and scattered photons. For the interaction between chiral molecules and light, the polarization of light generally plays a crucial role [17–19,26,30]. However, due to the interaction in Compton scattering being controlled by A^2, this results in the polarization vector of photons not entering the matrix element M, hence remaining uncoupled with the initial and final states of the electron. This observation is evident from Eqs. (15) and (18). Therein, the polarization information resides entirely in the term $|\boldsymbol{\epsilon}_1 \cdot \boldsymbol{\epsilon}_2|^2$, independent of the subsequent modulus squared. Particularly for the light-scattering spectrum, $|\boldsymbol{\epsilon}_1 \cdot \boldsymbol{\epsilon}_2|^2$ merely furnishes a function related to the direction of the scattered photon. Nevertheless, as Eq. (18) necessitates integration over the direction of the scattered photon, considering different polarizations may have certain effects on the momentum spectrum $\varphi(\boldsymbol{p})$. In addition, measuring the momentum of scattered photons is currently a highly challenging task, let alone measuring the polarization of scattered photons. Given these reasons, we do not intend to consider the polarization of incident photons and scattered photons in this paper, but rather average the polarization of the incident photons and sum the polarization of the scattered photons, that is,

$$|\boldsymbol{\epsilon}_1 \cdot \boldsymbol{\epsilon}_2|^2 \rightarrow (1 + \cos^2\theta). \quad (20)$$

Here, θ is the angle between $\boldsymbol{k}_1$ and $\boldsymbol{k}_2$.

C. Averaging orientation

If considering the average of space orientation, there is

$$\frac{d\sigma}{d\Omega_{\hat{k}_2}d\omega_2} = \frac{1}{8\pi^2} \int_0^{2\pi} d\alpha \int_0^{2\pi} d\gamma \int_0^{\pi} \sin\beta d\beta$$

$$\times (1 + \cos^2\theta) \frac{p\omega_2}{\omega_1} \sum_{l_2 m_2} \left| \sum_{(nlm)l_1 m_1 m'} D^l_{m'm} \mathscr{A} \mathscr{B} \right|^2. \quad (21)$$

Due to

$$\int_0^{2\pi} d\alpha \int_0^{2\pi} d\gamma \int_0^{\pi} \sin\beta d\beta D^{j_1*}_{m_1 k_1} D^{j_2}_{m_2 k_2}$$

$$= \frac{8\pi^2}{2j_1 + 1} \delta_{j_1 j_2} \delta_{k_1 k_2} \delta_{m_1 m_2}, \quad (22)$$

thus

$$\frac{d\sigma}{d\Omega_{\hat{k}_2}d\omega_2} = (1 + \cos^2\theta) \frac{\omega_2}{p\omega_1} \sum_{l_2 m_2} \sum_{(nlm)m'} \left| \sum_{l_1 m_1} \mathscr{C} \mathscr{D} \right|^2. \quad (23)$$

Here, we redefine two coefficients, with

$$\mathscr{C} = \sqrt{(2l_1 + 1)(2l_2 + 1)} \begin{pmatrix} l_2 & l_1 & l \\ 0 & 0 & 0 \end{pmatrix} \begin{pmatrix} l_2 & l_1 & l \\ -m_2 & m_1 & m' \end{pmatrix} \quad (24)$$

and

$$\mathscr{D} = i^{l_1} Y^*_{l_1 m_1}(\hat{\boldsymbol{k}}) \int_0^{\infty} F_{l_2}(r) R_{nlm}(r) j_{l_1}(kr) r dr. \quad (25)$$

By the way, in order to make the expression concise, we omit the constant factor in Eq. (23), which will not affect the qualitative results.

In addition, for the momentum spectrum, we obtain

$$\varphi(\boldsymbol{p}) = \int \frac{\omega_2}{\omega_1} (1 + \cos^2\theta) \sum_{(nlm)} \left(\frac{1}{2l+1} \right.$$

$$\times \sum_{m'} \left| \sum_{l_1 l_2 m_1 m_2} \mathscr{A} \mathscr{B} Y_{l_2 m_2}(\hat{\boldsymbol{p}}) \right|^2 \right) d\Omega_{\hat{k}_2}. \quad (26)$$

III. RESULTS

In Sec. II, we present the derivation of the light-scattering spectrum and ionization momentum spectrum in Compton scattering of chiral hydrogen. In this section, we will take two different types of chiral hydrogen as examples to show the corresponding numerical simulation results. For convenience, we might as well set the z axis along the direction of $\boldsymbol{k}_1$ in the following discussions. Meanwhile, the energy of the incident photon is set to a fixed value, i.e., $\omega_1 = 1.5$ keV.
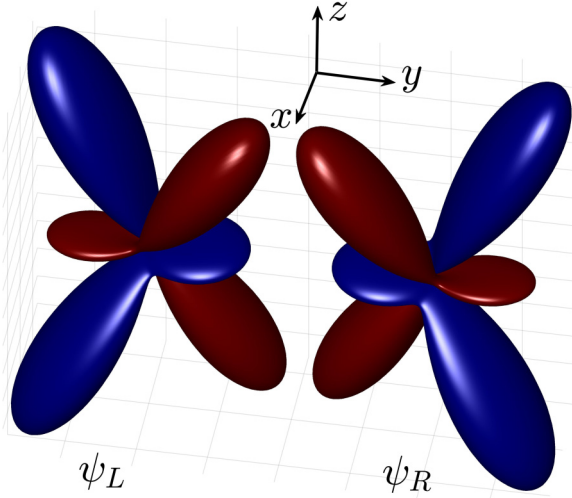
FIG. 1. The variation of the probability distribution $|\psi_{L/R}(r,\hat{\boldsymbol{r}})|^2$ [given by Eq. (27)] with respect to the solid angle as $r = 16$ a.u. Here, blue means $\psi_{L/R} < 0$, while red indicates the opposite.

A. The ρ-type chiral wave functions

Let us first discuss a so-called ρ-type chiral hydrogen [26], whose left- and right-handed wave functions can be written as

$$\psi_L = \tfrac{1}{2}R_{4d}(Y_{21} - Y_{2-1}) + \tfrac{1}{2}iR_{4f}(Y_{31} + Y_{3-1}),$$

$$\psi_R = \tfrac{1}{2}R_{4d}(Y_{21} - Y_{2-1}) - \tfrac{1}{2}iR_{4f}(Y_{31} + Y_{3-1}). \quad (27)$$

In the above equation, R_{nl} represents the radial wave function in the energy eigenstate of the hydrogen atom. Note that both ψ_L and ψ_R are real numbers. In order to demonstrate the chirality of such wave functions more intuitively, we present the spatial probability distributions of the left- and right-handed wave functions in Fig. 1. It is evident from the figure that ψ_L and ψ_R are mirror symmetric about the x-z plane and cannot be made to coincide through spatial rotation. For these two wave functions, we numerically simulate their corresponding light-scattering spectrum $d\sigma/d\Omega_{\hat{k}_2}$ by integrating ω_2 in Eq. (15). The specific results are shown in Fig. 2. Surprisingly, the light-scattering spectra for both are identical. Here, it is important to emphasize that the three Euler angles $(\alpha\beta\gamma)$ corresponding to the wave functions in Eq. (27) are all equal to 0. However, through our calculations, we find that even if α, β, and γ are changed arbitrarily, that is, the spatial orientation of the left- and right-handed wave functions is adjusted in any direction, the light-scattering spectra still exhibit no differences for ψ_L and ψ_R. This implies that in Compton scattering of ρ-type chiral hydrogen with any spatial orientation, the chirality cannot be determined from the light-scattering spectrum. As analyzed in Ref. [26], ρ-type chiral hydrogen can effectively simulate the electronic states of actual chiral molecules. Therefore, its Compton scattering may provide some qualitative insights into that of the latter. Unfortunately, our above results suggest that measuring the light-scattering spectral signal may not be a suitable approach when using Compton scattering to probe the chirality of molecules.

In view of the above, we may now consider focusing on an alternative signal—the momentum spectrum of ionized
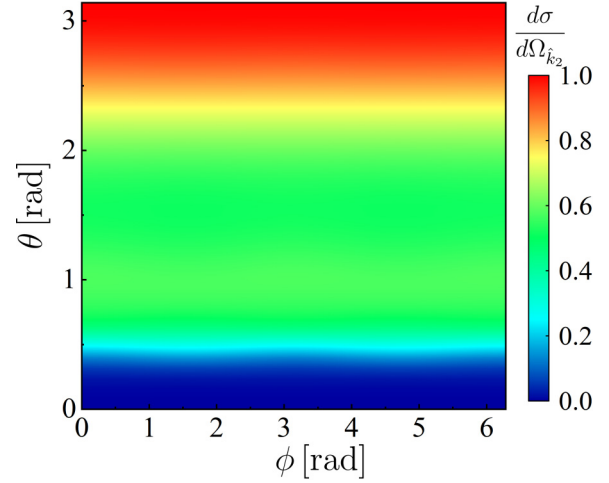

FIG. 2. The light-scattering spectrum obtained with the help of Eq. (27). Here, ϕ is the azimuth angle of $\boldsymbol{k}_2$. The data in the figure have been normalized such that the maximum value is 1.

electrons. As depicted in Fig. 3, we obtain the momentum spectrum of the ionized electron generated in Compton scattering of ρ-type chiral hydrogen through Eq. (18). By comparing Fig. 3(a) with Fig. 3(b) [or Fig. 3(c) with Fig. 3(d)], it is shown that, unlike the light-scattering spectra, the momentum spectrum is sensitive to chirality. To highlight this enantiosensitivity more clearly, we can quantify the differences between the signals of two enantiomers by defining a dissymmetry factor w, where

$$w = \frac{\varphi_L - \varphi_R}{\varphi_L + \varphi_R}. \quad (28)$$

For instance, Fig. 3(e) illustrates the difference between Figs. 3(a) and 3(b), and the results indicate an asymmetry of up to 24.2%. Meanwhile, we note that $\varphi_L(p_x, p_y, p_z) = \varphi_R(p_x, -p_y, p_z)$, that is, $\varphi_L(\boldsymbol{p})$ and $\varphi_R(\boldsymbol{p})$ also show mirror symmetry about the x-z plane. This suggests that the momentum spectrum might possess chirality as well. However, such evidence is insufficient to determine chirality definitively, as achiral three-dimensional (3D) distributions could also exhibit these characteristics.

Currently, there is no universal and single method to define the chirality of a 3D distribution [27,31,32]. For example, one could define a parameter [27,33]

$$\chi = \frac{\min_{\mathcal{R}} \int \left| \varphi_L^{\mathcal{R}}(\boldsymbol{p}) - \varphi_R(\boldsymbol{p}) \right| d\boldsymbol{p}}{\int \varphi_R(\boldsymbol{p}) d\boldsymbol{p}}. \quad (29)$$

Here, $\mathcal{R}$ represents Euler angles, and $\varphi_L^{\mathcal{R}}(\boldsymbol{p})$ denotes the result of performing an Euler rotation on $\varphi_L(\boldsymbol{p})$. Clearly, according to this definition, when $\chi = 0$, $\varphi(\boldsymbol{p})$ is achiral, whereas when $\chi \neq 0$, it exhibits chirality. However, considering the computational complexity involved, this method may not be practical. However, considering the actual computational effort here, this method is not practical. We might as well find another way. In fact, Fig. 3 displays 2D slices at various p_y values. Imagine that if these slices are put back into the 3D space, $\varphi_L(\boldsymbol{p})$ and $\varphi_R(\boldsymbol{p})$ cannot coincide by rotation. Hence, we can directly conclude that Compton scattering maps the
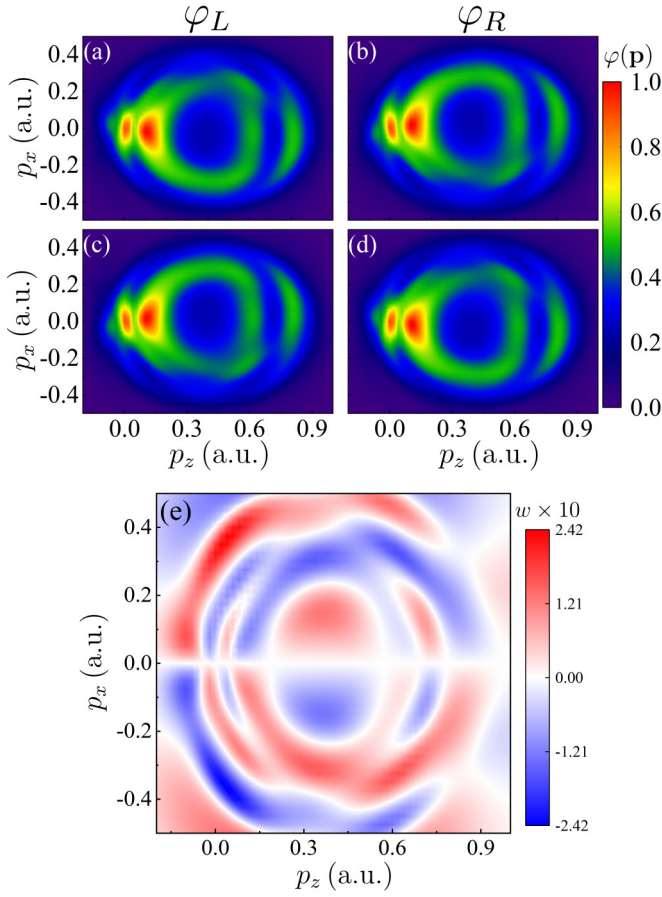
FIG. 3. 2D slices of the momentum spectrum obtained with the help of Eq. (27): (a) $p_y = 0.1$ a.u., (b) $p_y = 0.1$ a.u., (c) $p_y = -0.1$ a.u., (d) $p_y = -0.1$ a.u. (e) Distribution of dimensionless dissymmetry factor w at $p_y = 0.1$ a.u. Here, the normalization method of the data in (a)–(d) is consistent with that in Fig. 2.
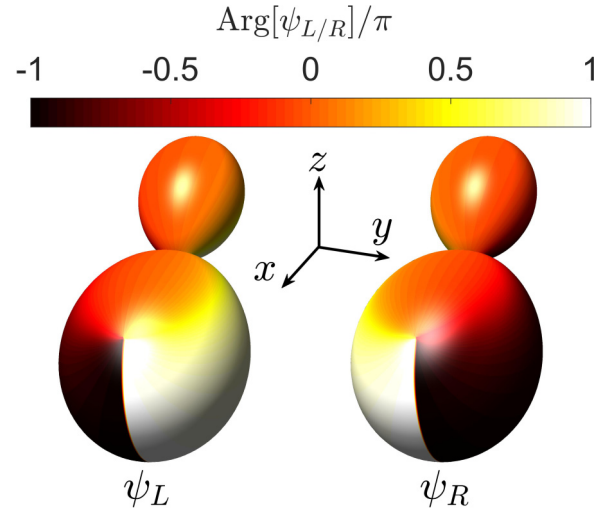

FIG. 4. The variation of the probability distribution $|\psi_{L/R}(r, \hat{r})|^2$ [given by Eq. (30)] with respect to the solid angle as $r = 2.1$ a.u. Here, color represents the magnitude of the phase of the wave function.

chirality features of the ρ-type chiral hydrogen into its corresponding ionization momentum spectrum.

In addition, it can also be observed from Fig. 3 that $\varphi_{L(R)}(p_x, p_y, p_z) = \varphi_{L(R)}(-p_x, -p_y, p_z)$. For this phenomenon, we may find an explanation from the wave functions satisfying $\psi_{L(R)}(x, y, z) = -\psi_{L(R)}(-x, -y, z)$ in Eq. (27). Of course, this explanation is a bit far-fetched here, but we will provide a more detailed argument for it in Sec. III B.

B. The sp^3 hybrid orbital

Now, we introduce another type of chiral hydrogen, and the corresponding left- and right-handed wave functions are given by

$$\psi_L = g_1 R_{2s} Y_{00} + R_{2p}(g_2 Y_{11} + g_3 Y_{10} - g_4 Y_{1-1}),$$

$$\psi_R = g_1 R_{2s} Y_{00} + R_{2p}(g_4 Y_{11} + g_3 Y_{10} - g_2 Y_{1-1}), \quad (30)$$

where $g_1 = 0.93$, $g_2 = 0.3/\sqrt{2}$, $g_3 = 0.3$, and $g_4 = 0.1/\sqrt{2}$. Such wave functions can represent the lowest-energy sp^3 hybrid orbitals in the simplest chiral molecule [34], and their spatial probability distribution is shown in Fig. 4. Clearly,

ψ_L and ψ_R still exhibit mirror symmetry about the x-z plane and are a pair of enantiomers. But it should be noted that the chirality here depends on the phase of the wave function, not the probability density.

Next, we can also define the dissymmetry factor W corresponding to the light-scattering spectra, that is,

$$W = \left(\left. \frac{d\sigma}{d\Omega_{\hat{k}_2}} \right|_{\psi_L} - \left. \frac{d\sigma}{d\Omega_{\hat{k}_2}} \right|_{\psi_R} \right) \Big/ \left(\left. \frac{d\sigma}{d\Omega_{\hat{k}_2}} \right|_{\psi_L} + \left. \frac{d\sigma}{d\Omega_{\hat{k}_2}} \right|_{\psi_R} \right). \quad (31)$$

It could be employed to quantitatively characterize the light-scattering spectral differences between two enantiomers. Obviously, for the ρ-type chiral hydrogen discussed in Sec. III A, $W = 0$. However, for ψ_L and ψ_R in Eq. (30), there are significant light-scattering spectral differences, as illustrated in Fig. 5. This phenomenon also holds true for other spatial orientations. Although we currently lack a fundamental theoretical understanding of why this is the case, the results obtained so far are intriguing and valuable. This is because it suggests that the phase of the wave function also plays an important role when investigating chirality using Compton scattering.

In addition, we still simulate the ionization momentum spectrum, and the outcome in Fig. 6(e) suggests that the momentum spectrum remains sensitive to chirality. In particular, by comparing Fig. 6 with Fig. 3, we observe that the characteristic feature $\varphi_{L(R)}(p_x, p_y, p_z) = \varphi_{L(R)}(-p_x, -p_y, p_z)$ does not exist in Fig. 6, while the chirality feature $\varphi_L(p_x, p_y, p_z) = \varphi_R(p_x, -p_y, p_z)$ remains intact. This, to some extent, corroborates our assertion in Sec. III A (see the penultimate sentence). Because, with regard to the chiral hydrogen discussed in this section, there exists no inherent special association between $\psi_{L(R)}(x, y, z)$ and $\psi_{L(R)}(-x, -y, z)$, hence the relationship between $\varphi_{L(R)}(p_x, p_y, p_z)$ and $\varphi_{L(R)}(-p_x, -p_y, p_z)$ is no longer special.
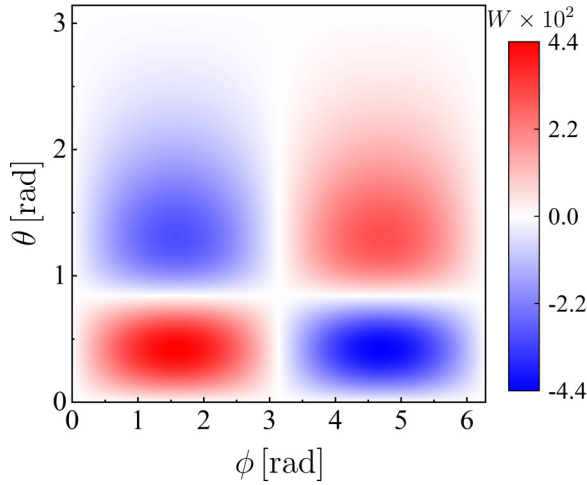
FIG. 5. Angular distribution of the dissymmetry factor W. The results are obtained with the help of Eq. (30).

Finally, let us briefly discuss the issue of orientation averaging, which is a general concern. For instance, the light-scattering spectrum is obtained through Eq. (23). We note that for the two types of chiral hydrogen discussed above,
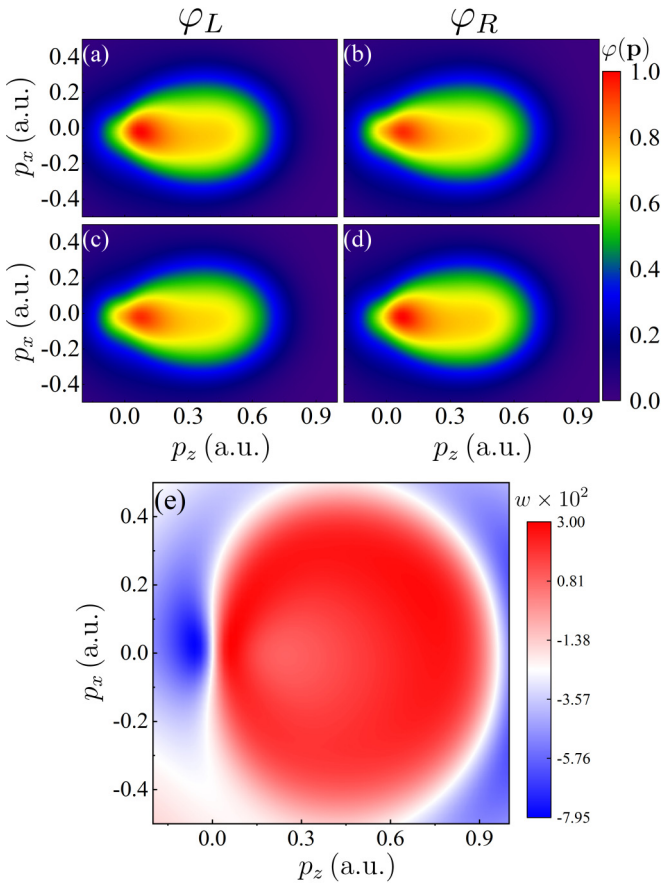

FIG. 6. 2D slices of the momentum spectrum obtained with the help of Eq. (30): (a) $p_y = 0.1$ a.u., (b) $p_y = 0.1$ a.u., (c) $p_y = -0.1$ a.u., (d) $p_y = -0.1$ a.u. (e) Distribution of dimensionless dissymmetry factor w at $p_y = 0.1$ a.u.

the difference between ψ_L and ψ_R lies in the different constant coefficients in $R_{nlm}(r)$ [see Eq. (5)]. Additionally, the summation over the index (nlm) in Eq. (23) occurs outside the modulus operation, and the modulus square term is independent of the magnetic quantum number m. Consequently, whether ψ_R or ψ_L is used for calculations, the light-scattering spectrum remains identical. Such a conclusion also applies to the momentum spectrum [see Eq. (26)].

IV. SUMMARY AND DISCUSSION

In summary, we have conducted a study on the Compton scattering of chiral hydrogen. Our aim is to demonstrate the differences in the response of two enantiomers to x rays during the process of Compton ionization. By considering two different types of chiral hydrogen as examples, our calculations regarding the dissymmetry factors indicate that there are significant distinctions between the ionization momentum spectrum corresponding to the two enantiomers. It is also found that the light-scattering spectra are incapable of chiral discrimination for ρ-type enantiomers with any specific spatial orientation. This outcome suggests there may be limitations in the application of Compton light-scattering spectra for enantiomeric recognition, despite its established effectiveness in investigating the momentum distribution of electrons in atoms or molecules.

Additionally, the wave functions of the chiral hydrogen employed in this paper are somewhat special, which also results in no chiral responses in the light-scattering spectra and the momentum spectrum when the enantiomers are isotropic. Nevertheless, we anticipate that the situation would vary for actual enantiomers with more complex wave functions. It should also be noted that experiments investigating chiral samples via Compton ionization are lacking. In fact, due to the maturity of COLTRIMS technique and the fact that the photon energy (1.5 keV in the present work) of the required x rays is not as high as demanded by the IA, we believe that relevant experiments should be feasible.

It should also be emphasized that the current Compton ionization method with the use of COLTRIMS still has many shortcomings, and it cannot completely replace the well-known electron momentum spectroscopy (EMS) [35] method, which has long been used for structural investigations in atomic and molecular physics. For example, the measurement of final photons in Compton scattering still faces significant difficulties, although indirect measurements could be achieved through coincidence measurement techniques [12]. Therefore, in the current context, this paper is just a simple attempt to apply Compton scattering to chiral discrimination, and we look forward to further theoretical and experimental explorations.

[1] J. Als-Nielsen and D. McMorrow, *Elements of Modern X-Ray Physics* (Wiley, Hoboken, NJ, 2011).

[2] M. F. C. Ladd, R. A. Palmer, and R. A. Palmer, *Structure Determination by X-Ray Crystallography* (Springer, Berlin, 1977), Vol. 233.

[3] M. J. Cooper, Compton scattering and electron momentum determination, Rep. Prog. Phys. **48**, 415 (1985).

[4] S. H. Glenzer and R. Redmer, X-ray Thomson scattering in high energy density plasmas, Rev. Mod. Phys. **81**, 1625 (2009).

[5] G. Dixit, O. Vendrell, and R. Santra, Imaging electronic quantum motion with light, Proc. Natl. Acad. Sci. USA **109**, 11636 (2012).

[6] G. Dixit, J. M. Slowik, and R. Santra, Proposed imaging of the ultrafast electronic motion in samples using x-ray phase contrast, Phys. Rev. Lett. **110**, 137403 (2013).

[7] A. H. Compton, A quantum theory of the scattering of x-rays by light elements, Phys. Rev. **21**, 483 (1923).

[8] A. H. Compton, The spectrum of scattered x-rays, Phys. Rev. **22**, 409 (1923).

[9] P. Eisenberger and P. M. Platzman, Compton scattering of x rays from bound electrons, Phys. Rev. A **2**, 415 (1970).

[10] P. Eisenberger, Electron momentum density of He and H_2; Compton x-ray scattering, Phys. Rev. A **2**, 1678 (1970).

[11] M. Kircher, F. Trinter, S. Grundmann, G. Kastirke, M. Weller, I. Vela-Perez, A. Khan, C. Janke, M. Waitz, S. Zeller, T. Mletzko, D. Kirchner, V. Honkimaki, S. Houamer, O. Chuluunbaatar, Y. V. Popov, I. P. Volobuev, M. S. Schoffler, L. P. H. Schmidt, T. Jahnke *et al.*, Ion and electron momentum distributions from single and double ionization of helium induced by Compton scattering, Phys. Rev. Lett. **128**, 053001 (2022).

[12] M. Kircher, F. Trinter, S. Grundmann *et al.*, Kinematically complete experimental study of Compton scattering at helium atoms near the threshold, Nat. Phys. **16**, 756 (2020).

[13] O. Chuluunbaatar, S. Houamer, Y. Popov, I. Volobuev, M. Kircher, and R. Dörner, Compton ionization of atoms as a method of dynamical spectroscopy, J. Quant. Spectrosc. Radiat. Transfer **272**, 107820 (2021).

[14] O. Chuluunbaatar, S. Houamer, Y. Popov, I. Volobuev, M. Kircher, and R. Dörner, Compton double ionization of the helium atom: Can it be a method of dynamical spectroscopy of ground state electron correlation? J. Quant. Spectrosc. Radiat. Transfer **278**, 108020 (2022).

[15] R. Dörner, V. Mergel, O. Jagutzki, L. Spielberger, J. Ullrich, R. Moshammer, and H. Schmidt-Böcking, Cold target recoil ion momentum spectroscopy: a momentum microscope to view atomic collision dynamics, Phys. Rep. **330**, 95 (2000).

[16] J. Ullrich, R. Moshammer, A. Dorn, R. Dörner, L. P. H. Schmidt, and H. Schmidt-Böcking, Recoil-ion and electron momentum spectroscopy: reaction-microscopes, Rep. Prog. Phys. **66**, 1463 (2003).

[17] L. D. Barron, *Molecular Light Scattering and Optical Activity*, 2nd ed. (Cambridge University Press, Cambridge, UK, 2004).

[18] G. D. Fasman, *Circular Dichroism and the Conformational Analysis of Biomolecules* (Springer, Berlin, 2013).

[19] P. J. Stephens, Theory of vibrational circular dichroism, J. Phys. Chem. **89**, 748 (1985).

[20] P. Herwig, K. Zawatzky, M. Grieser *et al.*, Imaging the absolute configuration of a chiral epoxide in the gas phase, Science **342**, 1084 (2013).

[21] D. Patterson, M. Schnell, and J. Doyle, Enantiomer-specific detection of chiral molecules via microwave spectroscopy, Nature (London) **497**, 475 (2013).

[22] D. Patterson and J. M. Doyle, Sensitive chiral analysis via microwave three-wave mixing, Phys. Rev. Lett. **111**, 023008 (2013).

[23] V. A. Shubert, D. Schmitz, D. Patterson, J. M. Doyle, and M. Schnell, Identifying enantiomers in mixtures of chiral molecules with broadband microwave spectroscopy, Angew. Chem., Int. Ed. **53**, 1152 (2014).

[24] D. Ayuso, O. Neufeld, A. Ordonez, P. Decleva, G. Lerner, O. Cohen, M. Ivanov, and O. Smirnova, Synthetic chiral light for efficient control of chiral light–matter interaction, Nat. Photon. **13**, 866 (2019).

[25] O. Neufeld, D. Ayuso, P. Decleva, M. Y. Ivanov, O. Smirnova, and O. Cohen, Ultrasensitive chiral spectroscopy by dynamical symmetry breaking in high harmonic generation, Phys. Rev. X **9**, 031002 (2019).

[26] A. F. Ordonez and O. Smirnova, Propensity rules in photoelectron circular dichroism in chiral molecules. I. Chiral hydrogen, Phys. Rev. A **99**, 043416 (2019).

[27] N. Mayer, S. Patchkovskii, F. Morales, M. Ivanov, and O. Smirnova, Imprinting chirality on atoms using synthetic chiral light fields, Phys. Rev. Lett. **129**, 243201 (2022).

[28] E. P. Wigner, *Group Theory: And its Application to the Quantum Mechanics of Atomic Spectra* (Academic, New York, 1959).

[29] F. Salvat and J. M. Fernández-Varea, Radial: A Fortran subroutine package for the solution of the radial Schrödinger and Dirac wave equations, Comput. Phys. Commun. **240**, 165 (2019).

[30] A. F. Ordonez and O. Smirnova, Propensity rules in photoelectron circular dichroism in chiral molecules. II. General picture, Phys. Rev. A **99**, 043417 (2019).

[31] A. B. Harris, R. D. Kamien, and T. C. Lubensky, Molecular chirality and chiral parameters, Rev. Mod. Phys. **71**, 1745 (1999).

[32] M. Petitjean, Chirality and symmetry measures: A transdisciplinary review, Entropy **5**, 271 (2003).

[33] O. Neufeld and O. Cohen, Unambiguous definition of handedness for locally chiral light, Phys. Rev. A **105**, 023514 (2022).

[34] P. Fischer, D. S. Wiersma, R. Righini, B. Champagne, and A. D. Buckingham, Three-wave mixing in chiral liquids, Phys. Rev. Lett. **85**, 4253 (2000).

[35] I. E. McCarthy and E. Weigold, Electron momentum spectroscopy of atoms and molecules, Rep. Prog. Phys. **54**, 789 (1991).